



HAL
open science

Functionalization of Carbon Nanotubes with Nickel Cyclam for the Electrochemical Reduction of CO₂

Silvia Pugliese, Ngoc Tran Huan, Jeremy Forte, Domenico Grammatico, Sandrine Zanna, Bao-Lian Su, Yun Li, Marc Fontecave

► **To cite this version:**

Silvia Pugliese, Ngoc Tran Huan, Jeremy Forte, Domenico Grammatico, Sandrine Zanna, et al.. Functionalization of Carbon Nanotubes with Nickel Cyclam for the Electrochemical Reduction of CO₂. ChemSusChem, 2020, 10.1002/cssc.202002092 . hal-03034395

HAL Id: hal-03034395

<https://hal.sorbonne-universite.fr/hal-03034395>

Submitted on 1 Dec 2020

HAL is a multi-disciplinary open access archive for the deposit and dissemination of scientific research documents, whether they are published or not. The documents may come from teaching and research institutions in France or abroad, or from public or private research centers.

L'archive ouverte pluridisciplinaire **HAL**, est destinée au dépôt et à la diffusion de documents scientifiques de niveau recherche, publiés ou non, émanant des établissements d'enseignement et de recherche français ou étrangers, des laboratoires publics ou privés.

1 **Functionalization of Carbon Nanotubes with Nickel Cyclam for the**
2 **Electrochemical Reduction of CO₂**

3

4 *Silvia Pugliese,^{1,2} Dr. Ngoc Tran Huan,¹ Jérémy Forte,³ Domenico Grammatico,^{2,4} Dr. Sandrine*
5 *Zanna⁵, Prof. Bao-Lian Su,² Yun Li,^{1*} Prof. Marc Fontecave^{1*}*

6

7 1. Laboratoire de Chimie des Processus Biologiques, UMR CNRS 8229, Collège de France-
8 CNRS-Sorbonne Université, PSL Research University, 11 Place Marcelin Berthelot, 75231
9 Paris Cedex 05, France.

10

11 2. Laboratory of Inorganic Materials Chemistry (CMI), University of Namur, 61 rue de Bruxelles,
12 B-5000 Namur, Belgium

13

14 3. Sorbonne Université, Institut Parisien de Chimie Moléculaire, UMR 8232 CNRS, 4 place
15 Jussieu, 75252 Paris Cedex 5, France

16

17 4. Bio-inspired Materials Group: Functionality & Self-assembly, Université de Pau et des Pays
18 de l'Adour, E2S UPPA, CNRS, IPREM UMR 5254, 64000, PAU, France

19

20 5. Chimie ParisTech-PSL Research University-CNRS, Institut de Recherche de Chimie Paris
21 (IRCP), 11 rue Pierre et Marie Curie, 75005 Paris, France

22

23 * to whom correspondence should be addressed : yun.xu-li@college-de-france.fr;
24 marc.fontecave@college-de-france.fr

25

26 **KEYWORDS:** CO₂ electroreduction; nickel cyclam; pyrene; heterogenization; carbon nanotubes

27

28 **Abstract**

29

30 The exploitation of molecular catalysts for CO₂ electrolysis requires their immobilization on the
31 cathode of the electrolyzer. As an illustration of this approach, a Ni-cyclam complex, with a
32 cyclam derivative functionalized with a pyrene moiety, was synthesized, shown to be a selective
33 catalyst for CO₂ electroreduction to CO and immobilized on a carbon nanotube-coated gas diffusion
34 electrode by using a non-covalent binding strategy. The as-prepared electrode is efficient, selective,
35 robust for electrocatalytic reduction of CO₂ to CO. Very high turnover numbers (ca. 61460) and
36 turnover frequencies (ca. 4.27 s⁻¹) were enabled by the novel electrode material in organic solvent-
37 water mixtures saturated in CO₂. This material provides an interesting platform for further
38 improvement.

39 Introduction

40

41 Catalysis for CO₂ electroreduction into energy-dense products, such as CO, formic acid,
42 hydrocarbons and alcohols, has attracted extensive research attention during the last 10 years as this
43 reaction represents one of the most promising strategies for both CO₂ utilization as a carbon source
44 and storage of intermittent renewable energy in the form of stable chemical energy. Catalysts are
45 needed to overcome important kinetic limitations related to the multi-electron and multi-proton
46 transfers associated with the CO₂ reduction reaction (CO₂RR). Current research focuses on both
47 heterogeneous materials^[1-3] and homogeneous organometallic complexes.^[4, 5] The former are
48 favored industrially due to more facile product separation and catalyst regeneration and recovery.
49 However, molecular compounds afford the opportunity to more easily design and synthetically tune
50 the coordination environment of the active metal center. Mechanistic studies are also facilitated in
51 that case. To reconcile these two approaches, homogeneous catalysts can be immobilized on
52 heterogeneous conductive supports to generate cathode materials for electrolyzers. Such
53 heterogenized molecular systems thus combine the advantages of a solid material (easy recovery of
54 products and catalysts, efficient electron transfer from the electrode support to the catalyst, high
55 Turnover Numbers) with those of molecular complexes (synthetic control of the electronic
56 properties and the coordination environment of the active sites), while suppressing deactivation
57 processes (such as dimerization) and solubility issues associated with the latter. This class of hybrid
58 catalysts for CO₂RR has been recently described in different review articles.^[6-8]

59 Among various methods, a widely used and straightforward technique for immobilizing molecular
60 catalysts is based on hydrophobic and π - π stacking interactions between a carbon-based support,
61 generally graphite electrodes or multi-walled carbon nanotubes (MWCNTs), and the molecular
62 catalyst, as recently reviewed.^[6-8] MWCNTs have the advantages of stability, high electrical
63 conductivity and high surface area. While there have been some successes regarding heterogeneous
64 immobilization of CO₂RR catalysts on carbon supports such as MWCNTs, these are few and
65 limited mainly to polyaromatic macrocyclic ligands.^[8] For example, immobilization of a CO₂RR
66 molecular catalyst is possible without any functionalization of the ligand when the ligand is highly
67 conjugated as in the case of metal porphyrins and phthalocyanines.^[9-11] In contrast, when the ligand,
68 such as bipyridine or benzene-based pincer derivatives, has a limited electronic delocalized
69 structure, an aromatic group, most often pyrene, has to be covalently added to the ligand: the pyrene
70 group allows tight grafting of the molecular complex on carbon electrode surfaces via π - π stacking
71 interactions. Regarding such simple ligands functionalized with a pyrene group, the most

72 representative reports concern bipyridine-pyrene derivatives used to immobilize a
73 [Re(bpy)(CO)₃Cl] complex on a graphite support^[12] or a [Mn(bpy)(CO)₃Br] complex on carbon
74 nanotubes^[13] as well as a pincer-pyrene ligand used to immobilize an Iridium complex onto a gas
75 diffusion electrode via carbon nanotubes.^[14] The three materials displayed interesting
76 electrochemical CO₂RR catalytic properties, however in some cases with limited activity and
77 stability.

78 In order to explore other classes of ligands, in particular non-aromatic in nature, and complexes
79 based on non-noble metals, we have investigated one of the most studied molecular catalysts for
80 CO₂RR, namely [Ni(cyclam)]²⁺ with cyclam = 1,4,8,11-tetraazacyclotetradecane. To our
81 knowledge, while the heterogenization of [Ni(cyclam)]²⁺ complex has already been proposed,^[15, 16]
82 there is no precedent for its non-covalent immobilization on a carbon-based nanostructured
83 electrode. For that purpose, we have synthesized an original pyrene-cyclam derivative and the
84 corresponding Ni complex, complex **1** in Scheme 1, which was found to be a unique 6-coordinated
85 Ni cyclam complex. We report here the electrocatalytic properties of complex **1** both in solution and
86 after immobilization on MWCNTs. The complex proved to behave as a very selective
87 homogeneous catalyst for CO₂ electroreduction to CO in organic solvents in the presence of water.
88 Furthermore, the presence of a pyrene moiety on the ligand was exploited to readily heterogenize
89 the complex on MWCNTs via non-covalent interactions. The novel hybrid solid electrode, obtained
90 by deposition of the functionalized MWCNTs on a Gas Diffusion Layer, was found to be active,
91 stable and highly selective for CO₂ electroreduction to CO in acetonitrile-water solvent. These
92 results illustrate the potential of immobilized molecular catalysts for CO₂ electroreduction, a class
93 of materials yet to be developed for such an application.

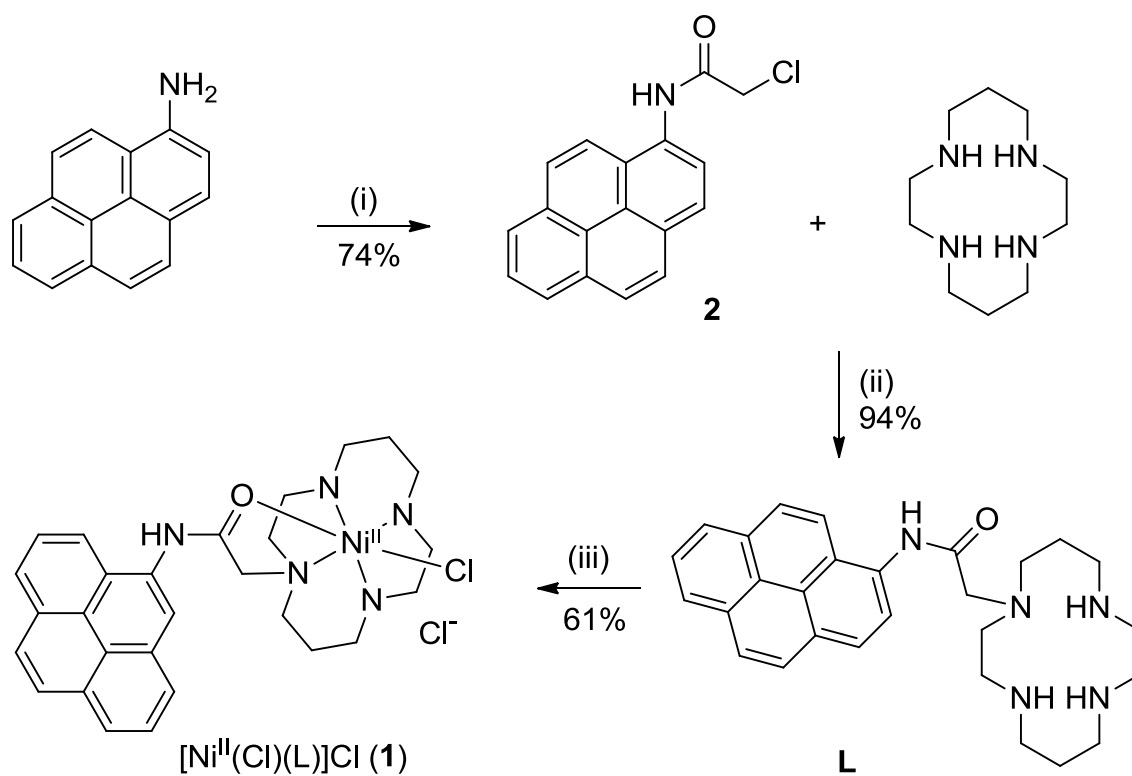
94

95 **Results**

96

97 *Complex synthesis and characterization*

98



99

100 **Scheme 1.** Synthesis of complex **1**. Conditions: (i) ClCH_2COCl , NEt_3 , CH_2Cl_2 ; (ii) K_2CO_3 , KI
 101 (cat.), CH_3CN ; (iii) $\text{NiCl}_2 \cdot 6\text{H}_2\text{O}$, EtOH .

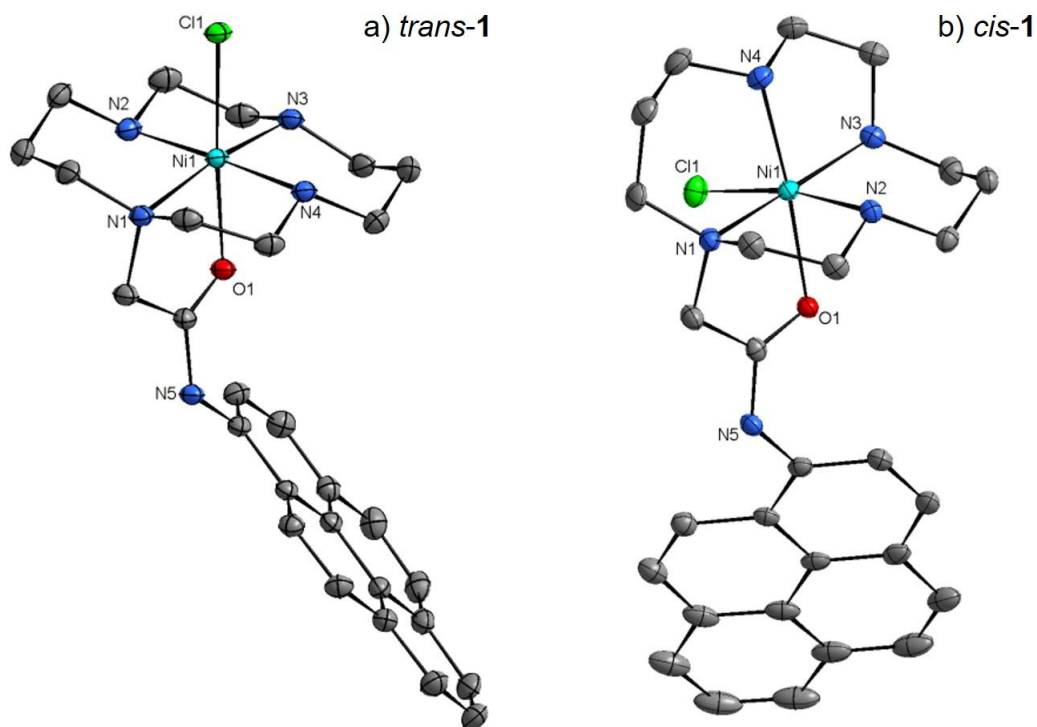
102 In order to synthesize a $[\text{Ni}(\text{cyclam})]^{2+}$ complex bearing a pyrene group, we chose to prepare the
 103 ligand **L**, in which one N atom of the cyclam ring is alkylated with a substituent containing a pyrene
 104 moiety (Scheme 1), according to a previously reported procedure.^[17] However, this previous
 105 synthesis gave the product in low yields and required arduous chromatographic purification. In this
 106 work, we improved the experimental procedure, especially for the N-alkylation of the cyclam ring
 107 step, by replacing the chromatographic purification step with washing with water, and **L** could be
 108 easily synthesized on a large scale. The corresponding nickel complex $[\text{Ni}^{\text{II}}(\text{Cl})(\text{L})](\text{Cl})$ (**1**) was
 109 obtained using nickel chloride hexahydrate in ethanol for metallation.

110 Complex **1** was isolated in the form of crystals suitable for X-ray analysis. Crystal data of all
 111 obtained structures are available in Table S1. Four different solvents, ethanol (EtOH), acetonitrile
 112 (CH_3CN), dichloromethane (CH_2Cl_2) and *N,N*-dimethylformamide (DMF) were used for
 113 crystallization, resulting in different crystal packings differentially stabilized by intermolecular
 114 hydrogen bonding, π -stacking and Van der Waals interactions (Table S1). In all structures, the
 115 nickel center ion was found in a distorted octahedral coordination geometry, with a chloride ion and
 116 the oxygen atom of the amide carbonyl group occupying two ligand positions and completing the
 117 four coordinating nitrogen atoms of the cyclam ring. However, two different structures, with

118 different configurations, were obtained, reflecting the presence of two isomers, named *trans-1* and
119 *cis-1* in the following. Four crystal structures of *trans-1* and two crystal structures of *cis-1* were
120 solved (Tables S1 and S2). In *trans-1*, which crystallized in all solvents used, Cl and O ligands
121 occupy the axial positions and are thus *trans* to each other with respect to the Ni ion, while the four
122 positions of the equatorial plane are occupied by the N atoms of the cyclam ring (Figure 1a). For the
123 *cis-1* isomer, which crystallized in EtOH and DMF, Cl and O ligands are *cis* to each other: the
124 equatorial plane is constituted by three N atoms of the cyclam ring (two secondary and one tertiary
125 amines) and a Cl ligand while the apical positions are occupied by the O atom of the amide
126 carbonyl group and the fourth N atom (one secondary amine) of the cyclam ring (Figure 1b). In the
127 two isomers, the nickel ion, the tertiary nitrogen atom and the carbonyl oxygen atom are together
128 part of a five-membered ring with two carbons from the dangling substituent (Figure 1). Each
129 isomer is a racemic mixture of two enantiomers (only the *R,S,S,R trans-1* and the *S,S,S,S cis-1* are
130 shown in Figure 1).

131 Bond lengths and angles values for all obtained crystal structures are given in Table S2. The Ni-O
132 bond lengths are in the range of those of Ni-N (between 2.05 and 2.14 Å), while the Ni-Cl bond
133 lengths (between 2.40 and 2.45 Å) are slightly longer. All these values are close to those of a
134 similar octahedral [Ni(cyclam)(OH₂)(Cl)]Cl complex, previously reported by Zhanaidarova and al
135 (Ni-O distance : 2.17 Å and Ni-Cl distance : 2.52 Å).^[16]

136



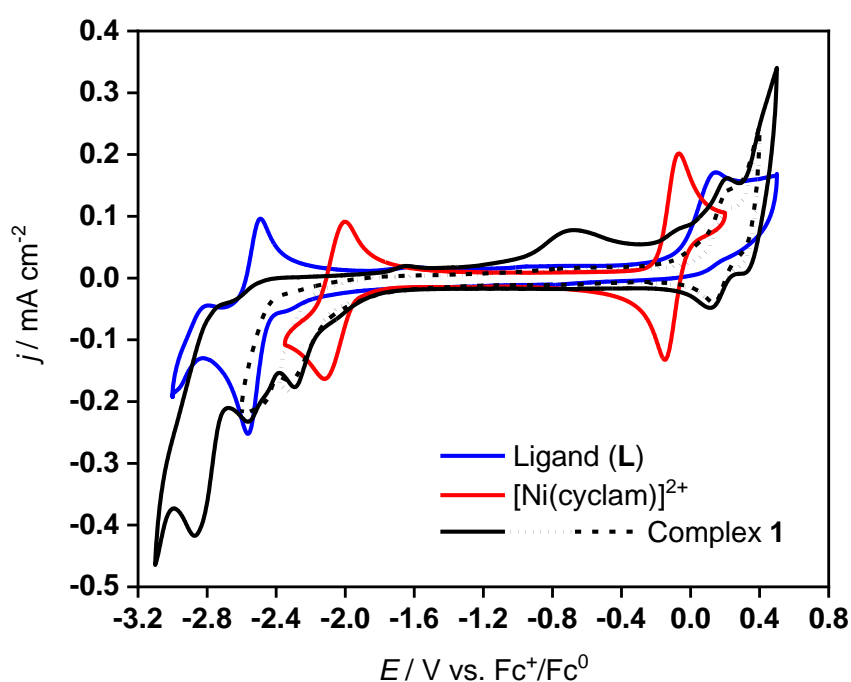
137

138 **Figure 1.** Crystal structure representation of the cation part of complex **1**. Ellipsoids are drawn with
139 30% probability. All hydrogen atoms are omitted for the sake of clarity. (a) *R,S,S,R trans-1* (from
140 crystallization in CH₃CN); (b) *S,S,S,S cis-1* (from crystallization in DMF). Only one of the
141 enantiomers is shown in both cases.

142
143 The electrochemical properties of complex **1** were studied in DMF, with all potentials vs. Fc⁺/Fc⁰.
144 Figure 2 (dotted, dashed and black) shows the complex cyclic voltammograms (CVs) of complex **1**
145 (1 mM) in DMF with 0.1 M TBAPF₆ as a supporting electrolyte on a glassy carbon disk (3 mm
146 diameter) as a working electrode, under an argon atmosphere, when scanned down to either -2.38, -
147 2.62 or -3.1V. The complexity comes from the fact that two different complexes, *trans-1* and *cis-1*,
148 are present in solution and that the ligand itself is redox-active due to the presence of pyrene.^[18] The
149 first feature at -2.28 V was assigned to the one-electron reduction of Ni^{II} to Ni^I, approximately 180
150 mV more cathodic than for the unfunctionalized [Ni(cyclam)]²⁺ complex peaking at -2.1 V (Figure
151 2, red), in agreement with a much more electron-enriched Ni center in complex **1** due to the
152 presence of extra electron-donating ligands. As a confirmation of this assignment to the metal site,
153 this feature was absent on the CV of the unmetallated pyren-cyclam ligand, **L** (Figure 2, blue). This
154 signal is irreversible in all CVs even when reversing the scan immediately after the reduction peak,
155 in contrast to that of [Ni(cyclam)]²⁺ (Figure 2). This indicates de-coordination of Cl or/and O
156 ligands upon reduction. Quite often, a small shoulder was present at -2.1 V, likely corresponding to
157 a very small amount of the complex without Cl/O coordination, likely in equilibrium with complex
158 **1** in solution. A second complex irreversible feature appeared at slightly more cathodic potential
159 (from -2.38 to -2.65 V) and proved difficult to assign. It could possibly have contributions in part
160 from the one-electron reduction of the pyrene ring, even though the pyren-cyclam ligand, **L**,
161 exhibits a reversible signal in this potential region (Figure 2, blue). Finally, upon scanning down to
162 below -3.0 V, a signal at -2.86 V was observed and assigned to Ni^I to Ni⁰ reduction. This signal is
163 indeed absent within the CV of the unmetallated pyrene-cyclam ligand and is also present in the CV
164 of [Ni(cyclam)]²⁺ upon scanning at a potential (- 2.55 V) allowing Ni^I to Ni⁰ conversion (Figure
165 S1). On the oxidizing return scan, the feature at + 0.2 V, also found in the unmetallated pyrene-
166 cyclam ligand, is assigned to ligand oxidation (Figure 2). The broad signal at -0.66 V was
167 exclusively seen after scanning down to a very negative potential, and not when the cathodic scan
168 was reversed after the second reduction wave at - 2.62 V. This is consistent with Ni⁰ species
169 generated at negative potentials and adsorbing on the surface of the electrode where they get
170 oxidized to Ni^{II} at -0.66 V during the back scan. A similar situation was observed with the

171 unfunctionalized $[\text{Ni}(\text{cyclam})]^{2+}$ complex when scanning down to very negative potentials (Figure
172 S1).

173 The cathodic peak current density (j_p) at -2.28 V varied linearly with the square root of the scan rate
174 ($v^{1/2}$) from 0.01 to 0.5 Vs^{-1} under Ar, consistent with diffusion-controlled processes and thus with
175 active complex **1** remaining in solution (Figure S2). We also verified that no adsorption of the
176 complex occurred at the surface of the GC electrode. Indeed, when, after 30 cycles of CV, the
177 electrode was removed from the electrolyte and used in a fresh electrolyte without complex **1**, no
178 signal corresponding to complex **1** could be observed in the CV.



179

180 **Figure 2** Cyclic voltammograms of complex **1** (black, dashed and dotted), $[\text{Ni}(\text{cyclam})]^{2+}$ (red),
181 ligand (**L**, blue). Conditions: DMF with 0.1M TBAPF_6 as the electrolyte, under Ar and at room
182 temperature. Concentrations were 1 mM for all species. Scan rate 100 mV s^{-1} .

183

184 *CO_2 reduction catalyzed by complex 1*

185

186 Upon addition of CO_2 , in the absence of a source of protons, the CV of 1 mM complex **1** (Figure
187 S3) presented a small catalytic wave with an increase of current density and a potential at half-peak
188 catalytic current of about -2.16 V, more anodic that of the $\text{Ni}^{\text{II}} / \text{Ni}^{\text{I}}$ signal and with an onset

189 potential close to that of $[\text{Ni}(\text{cyclam})]^{2+}$. In line with previous reports on CO_2 electroreduction
190 catalyzed by $[\text{Ni}(\text{cyclam})]^{2+}$, this wave is assigned to the catalytic reduction of CO_2 to CO during
191 which reduction of Ni^{II} to Ni^{I} promotes de-coordination of Cl/O ligands and allows Ni^{I} to bind and
192 activate CO_2 within a liberated coordination site.^[19]

193 However, given the importance of protons in the CO_2RR in general and specifically for CO_2RR
194 catalyzed by $[\text{Ni}(\text{cyclam})]^{2+}$,^[20] the effect of increased concentrations of H_2O was studied by CV
195 and bulk electrolysis. As expected, the catalytic current increased further upon addition of H_2O ,
196 from 0.4 M to 2 M (Figure S4a). Considering a CO/CO_2 reduction potential in a DMF–water
197 solvent mixture at - 1.41 V vs. Fc^+/Fc^0 (CO/CO_2 potential is reported to be - 0.690 V vs. NHE^[21]
198 and the Fc^+/Fc^0 potential is reported to be 0.720 V vs. NHE in DMF,^[22] the observed onset potential
199 at -1.95 V corresponds to an overpotential of about 540 mV. In the absence of CO_2 , a catalytic
200 current, assigned to proton reduction to hydrogen, also increased upon increasing the concentration
201 of H_2O (Figure S4b), however with an onset potential more cathodic than that for CO_2 reduction.
202 This reflects the greater potential of complex **1** to catalyze the reduction of CO_2 . Catalysis was
203 similarly stimulated when using 2,2,2-Trifluoroethanol (TFE) as a proton source (Figure S5). In the
204 following, only H_2O was considered as the proton source.

205 A controlled-potential electrolysis (CPE) was then carried out at -2.39 V during which reaction
206 products were analyzed and quantified, either by gas chromatography (for CO and H_2), by Ionic
207 Exchange Chromatography (for HCOOH) and ^1H NMR (for CH_3OH). For that purpose, the
208 electrochemical cell used a 1 cm^2 GC plate as the working electrode and the electrolyte was a
209 solution of complex **1** (1 mM) in CO_2 -saturated DMF containing 0.1 M TBAPF_6 and 2 M H_2O as a
210 proton source. CVs obtained with such a cell reproduced nicely the above CVs (Figure S6a). After
211 60 minutes electrolysis (Figure S6b), CO was found as the only reaction product in the gaseous
212 phase (faradaic yield: 96%) and no formate could be detected in the liquid phase. The catalyst
213 proved quite robust during 1 hour electrolysis as shown from the stability of the current density,
214 while its activity is limited as shown by the low current density ($0.3\text{ mA}\cdot\text{cm}^{-2}$). As a further proof of
215 the stability of the catalyst, a CV recorded after CPE was found to be comparable to that before
216 electrolysis, except for a small decrease in intensity (Figure S6a). The same experiment but in the
217 absence of complex **1** did not yield any CO_2 reduction products.

218

219 *Immobilization of complex 1: preparation of the hybrid electrode and characterization*

220

221 Complex **1** was immobilized on MWCNTs through the establishment of π - π stacking interactions
222 between the pyrene moieties and graphene motifs. In the first step, MWCNTs (2 mg) were first
223 sonicated in ethanol in the presence of Nafion, then drop-casted on a 1 cm² surface of commercial
224 gas diffusion layer (GDL), consisting of a carbon fibres cloth coated with a micro-porous Teflon
225 layer embedding carbon black so as to keep electronic conductivity properties. Then the
226 MWCNT/GDL electrode was dipped into a solution of 10 mM complex **1** in DMF, left overnight
227 and then washed with water and acetonitrile to remove any loosely bound complexes, and finally
228 air-dried before electrochemical experiments.

229 The **1**/MWCNT/GDL electrode was characterized by Scanning Electronic Microscopy (SEM) and
230 X-ray photoelectron spectroscopy (XPS). As shown in Figure S7a, a porous network of MWCNTs
231 was observed in SEM images after functionalization. XPS analysis (survey spectrum) confirms the
232 presence of Ni and N atoms, from complex **1**, on the surface of the electrode, together with O atoms
233 from alcohol or carboxylic acid defects of pristine MWCNTs (Figure S8 and Table S3). A Ni 2p_{3/2}
234 signal is observed at 855.9 eV in good agreement with the presence of a Ni^{II} ion. Since there is
235 fluoride in the deposited materials coming from Nafion with the F auger peak masking the Ni 2p
236 signal at 861.47 eV, a control MWCNT/GDL electrode in the absence of complex **1** has been also
237 analysed by XPS. The peak decomposition allowed to identify the signal of Ni 2p (Figure S8 and
238 Table S1) and the ratio of N/Ni is 4.5 approximately, whereas the N 1s peak was centered at 400.4
239 eV.

240 The **1**/MWCNT/GDL electrode was also characterized by Cyclic Voltammetry. CVs were recorded
241 in CH₃CN containing 0.1M TBAPF₆, using such **1**/MWCNT/GDL electrode (Figure S9). The high
242 capacitive currents observed in the voltammograms are explained by the 3D structure and the high
243 surface area of the working electrodes. Integration of the signal at - 1.7 V vs. Fc⁺/Fc⁰
244 corresponding to Ni reoxidation from Ni^I to Ni^{II} allowed to determine a concentration of
245 electroactive species for the complex of 5 10⁻⁹ mol cm⁻² (see experimental section). Such a value is
246 in line with previously reported values for MWCNTs functionalized with molecular Ni
247 complexes.^[23] The intensity of that peak was directly proportional to the scan rate, thus confirming
248 the immobilization of the nickel complex onto the electrode surface (Figure S9).

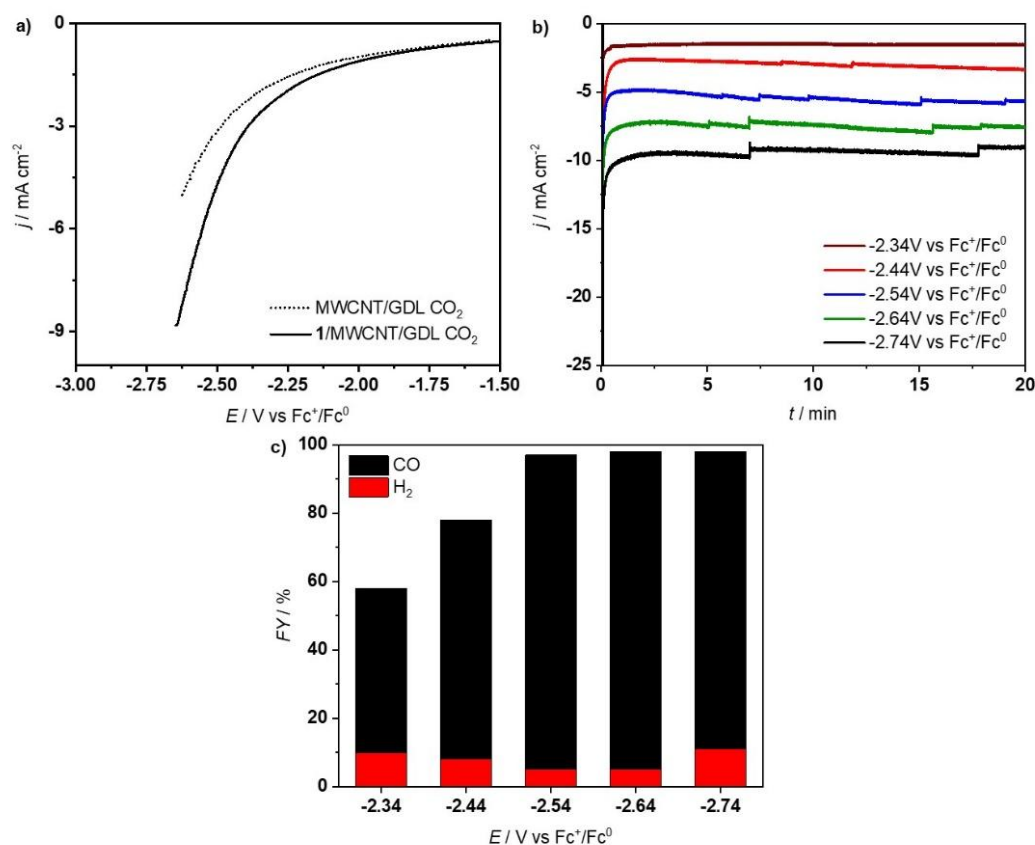
249

250 *Immobilization of complex 1: electroreduction of CO₂.*

251

252 The electrochemical reduction of CO₂ using the new electrode material was carried out in CH₃CN
253 containing 0.1M TBAPF₆ as the electrolyte, in the presence of 1% H₂O as a proton source, after

254 saturation with CO₂. A linear sweep voltammogram (LSV) shows a catalytic wave occurring at
 255 more anodic potentials as compared to the MWCNT/GDL control electrode (Figure 3a).
 256 Chronoamperometric measurements were carried out at various potentials from - 2.34 to - 2.74 V
 257 vs. Fc⁺/Fc⁰ for 20 min (Figure 3b). The current density proved stable in all cases. As a matter of
 258 fact, the same electrode could be used for several independent electrolysis experiments without any
 259 loss of activity. The CO₂ reduction products distribution, in terms of faradaic yields (FY), is shown
 260 in Figure 3c. CO was the major product at all potentials, with the highest FY value (92%) obtained
 261 at - 2.54 V vs. Fc⁺/Fc⁰ (with a current density of 6 mA.cm⁻²). In all cases H₂ accounted for less than
 262 11% and no formate could be detected. As a control experiment, CPE using a MWCNT/GDL
 263 electrode was performed at - 2.54 V vs. Fc⁺/Fc⁰ during 20 min (Figure S10a). Not only the current
 264 density was much lower (2.3 mA.cm⁻²) but the system was selective for H₂ production instead (FY=
 265 83% with a FY for CO of 4%). As a further control experiment, a CPE of 1/MWCNT/GDL at -
 266 2.54 V vs. Fc⁺/Fc⁰ was also run under Ar (Figure S10b). Only H₂ was produced after 20 min with
 267 no detectable CO₂ reduction products. Finally, CPE experiments were carried out at - 2.54 V vs.
 268 Fc⁺/Fc⁰ for 20 min with increased amounts of water (3% and 5%). As expected, the system became
 269 much less selective for CO₂ reduction, leading to FY for CO of only 22% and 12%, respectively.



270

271 **Figure 3.** (a) LSV of **1**/MWCNT/GDL (black) and MWCNT/GDL (dotted) in acetonitrile with
272 TBAPF₆ 0.1 M and H₂O 1% under CO₂. Scan rate 10 mV s⁻¹. (b) Controlled Potential Electrolysis
273 using **1**/MWCNT/GDL as the electrode at different potentials under the same conditions. (c)
274 Faradaic yields for CO and H₂ after 20 min electrolysis at different potentials.

275 A longer experiment (4h) carried out at - 2.54 V vs. Fc⁺/Fc⁰ using the **1**/MWCNT/GDL electrode
276 under CO₂ confirmed the stability of the catalytic material as well of its selectivity with a FY for
277 CO of more than 90% after 4h electrolysis (Figure S11). SEM (Figure S7b) as well as XPS (Figure
278 S12) analysis after 4h electrolysis showed no substantial change in the structure of the electrode. In
279 the XPS spectrum, the Ni 2p signal was identical to that before electrolysis (Figure S12c). The
280 decomposition of N1s also confirmed the presence of cyclam (N 1s signal at 400.3 eV), while an
281 additional signal was observed at around 403 eV, typical of quarternary ammonium such as TBA
282 present in the electrolyte. The ratio of N/Ni was 4.05 approximately, close to the value before
283 electrolysis.

284 Based on the amount of electroactive sites on the surface of the electrode (5 10⁻⁹ mol cm⁻²), a
285 remarkable Turnover Number for CO formation of 61460 was obtained after 4 h electrolysis,
286 corresponding to a Turnover Frequency value of 4.27 s⁻¹.

287

288 Discussion

289 For the sake of immobilizing a [Ni(cyclam)]²⁺ complex at the surface of an electrode, a novel
290 cyclam derivative carrying a pyrene moiety has been readily synthesized. This class of complex has
291 been chosen not only because [Ni(cyclam)]²⁺ is known to be a good, stable and selective molecular
292 catalyst for CO₂ electroreduction and it is based on a non-noble metal but also because, to our
293 knowledge, there is only one precedent for carbon electrode surface modification with
294 [Ni(cyclam)]²⁺ [16]. A [Ni(cyclam)]²⁺ complex modified with a carboxylic acid group was used to
295 for grafting onto titanium(zirconium) oxide surfaces but the resulting material was only studied for
296 its properties in photoelectron transfer.^[15] The new complex **1** is a 6-coordinated Ni complex, in
297 which the tetranuclear N-based coordination of the cyclam ring is completed by a chloride anion
298 and the oxygen atom of the amide group of the dangling substituent, with two different
299 configurations, *trans* and *cis*, with respect to the relative positions of the Cl and O ligands.
300 Coordination to a Ni^{II} center by the oxygen atom of a pendant amide group has been recently
301 reported in the case of substituted cyclen complexes of Ni^{II}.^[24] Complex **1** is thus the first
302 [Ni(cyclam)]²⁺ complex carrying a pyrene substituent.

303 Characterization of the electrochemical properties of complex **1** in DMF/H₂O using a glassy carbon
304 electrode has revealed the following features. First, upon one-electron reduction of Ni^{II} to Ni^I, the
305 complex enjoys decoordination of the Cl/O ligand(s); this is very important since the Ni^I state is the
306 active species for CO₂ binding and activation, a process that requires a free Ni coordination site.
307 Second, catalysis for CO₂ electroreduction occurs at the Ni^{II} / Ni^I redox process, as shown by cyclic
308 voltammetry, which indicates that the mechanism of the reaction catalyzed by complex **1** follows
309 that of [Ni(cyclam)]²⁺.^[25] Third, as in the case of [Ni(cyclam)]²⁺ CO₂ reduction catalyzed by
310 complex **1** is very selective for CO production (FY = 96%). Fourth, as expected, the activity is quite
311 weak, providing only small current densities; indeed, [Ni(cyclam)]²⁺ has been shown to be poorly
312 catalytically active when using a glassy carbon electrode, while the best activities were obtained
313 using a mercury electrode, on which the complex adsorbs and enjoys an increased reactivity both in
314 organic and aqueous electrolytes.^[19, 20, 26]

315 The pyrene-modified complex **1** has been immobilized on carbon nanotube-coated gas diffusion
316 electrode using a non-covalent approach and the novel electrode, **1**/MWCNT/GDL, has been
317 characterized electrochemically for CO₂ electroreduction. Under such an heterogenized
318 configuration, complex **1** retained its high selectivity for CO production (FY above 90%), with H₂
319 accounting for less than 15%. More interestingly, it was shown to be much more active in the
320 immobilized form than under homogeneous conditions: current densities up to 10 mA.cm⁻² could be
321 obtained as compared to 0.3 mA.cm⁻² for a 1 mM solution of complex **1**. Finally, the derivatized
322 electrode proved highly stable leading to impressive turnover numbers (61460 after 4 h
323 electrolysis). This is remarkable since the electrode support is carbon-based and not mercury, so far
324 the best electrode material for CO₂ electroreduction catalysed by [Ni(cyclam)]²⁺: this might indicate
325 that the stable interaction between complex **1** and the carbon surface of the MWCNTs specifically
326 favors the most reactive conformations of the complex and disfavors CO poisoning, CO desorption
327 being the turnover-limiting step of the catalytic cycle, as does mercury for the soluble
328 [Ni(cyclam)]²⁺ complex.^[20, 26] As a consequence, complex **1** is one of the very best molecular
329 catalysts, after immobilization onto an electrode surface, reported so far for CO₂ electroreduction,
330 as discussed below.

331 The only previous attempt to graft a [Ni(cyclam)]²⁺ complex on a solid electrode (in that case a
332 covalent grafting onto a glassy carbon electrode) was achieved by Kubiak and coworkers, using
333 electrooxidation of a terminal alkyne attached to the cyclam ring.^[16] This led to a cathode material
334 which proved poorly active (with current densities below 1 mA.cm⁻²) and poorly selective for CO₂
335 reduction to CO (FY_{CO} = 7%; FY_{H₂} = 89 %) under potential and solvent conditions comparable to

336 those used here. The present work thus represents a great improvement regarding the utilization of
337 solid electrodes functionalized with $[\text{Ni}(\text{cyclam})]^{2+}$. This is due in great part to the large surface
338 area and the nanostructuring of the CNTs support which allow a greater density of electroactive
339 species. As a matter of fact, the 1/MWCNT/GDL electrode is also much more efficient for CO_2
340 reduction to CO than a glassy carbon electrode functionalized with a $[\text{Re}(\text{bpy})(\text{CO})_3\text{Cl}]$ complex
341 using the same pyrene-dependent approach: the latter could achieve only 58 TONs during 1 hour
342 electrolysis, after which the activity was lost.^[12] Finally, the 1/MWCNT/GDL electrode compares
343 well with and complements the carbon nanotube-coated gas diffusion electrode derivatized with a
344 molecular iridium pincer dihydride catalyst, which allows high TONs (200000 in 8 hours) of
345 formate with high selectivity (> 90%) from CO_2 electroreduction in aqueous electrolytes.^[14] While
346 based on a noble metal, the latter is a reference material with respect to carbon electrodes
347 functionalized with a molecular catalyst for CO_2 reduction. Indeed, while $[\text{Mn}(\text{bpy})(\text{CO})_3\text{Br}]$ was
348 also attached to MWCNTs via π - π interactions of a pyrene group, present in a bpy ligand
349 derivative, with the CNT sidewalls, the resulting material proved much less active (low current
350 densities), less stable, less selective (giving a mixture of CO and HCOOH together with H_2 as the
351 major product) and achieving TONs of about 1500 after 8 h electrolysis under aqueous
352 conditions.^[13]

353 In conclusion, the present study confirms the benefits of incorporation of molecular catalysts onto
354 electrode surfaces using the pyrene-CNT approach for CO_2 electroreduction. More specifically, it
355 shows that the $[\text{Ni}(\text{cyclam})]^{2+}$ complex provides an excellent platform on which further
356 improvements of hybrid electrodes can be brought.

357

358 **Experimental Section**

359 *General*

360 All starting materials were commercially available (Sigma and TCI) and were used without further
361 purification. Solvents were purified by an MBRAUN SPS-800 Solvent Purification System. All
362 reactions were carried out under air atmosphere unless specified. ^1H and NMR spectra were
363 recorded on a Bruker Avance-III 300 NMR spectrometer (300 MHz) at room temperature. UV-Vis
364 spectra were recorded using a Cary 100 UV-Vis spectrophotometer instrument (Agilent).

365

366 *Synthesis of Complex I*

367 **2-Chloro-*N*-pyren-1-yl-acetamide (2)**. The synthesis was carried on as previously described with
368 slight modifications.^[27] Under an Ar atmosphere, 1-aminopyrene (5.45 g, 25.1 mmol) and
369 triethylamine (5.6 mL, 40.1 mmol) were dissolved in CH₂Cl₂ (500mL), and chloroacetyl chloride
370 (2.8 mL, 35.1 mmol) was added dropwise via a syringe. After 12 h of stirring under Ar, the
371 precipitate was filtered, washed with H₂O and cold CH₂Cl₂ several times. The crude product was
372 dried under vacuum over night to yield the product as a pale-grey powder which was used for the
373 next step without further purification (5.49 g, 74%). ¹H NMR (CDCl₃, 300 MHz) δ 9.01 (br s, 1H),
374 8.45 (d, *J* = 8.3 Hz, 1H), 8.21-8.14 (m, 4H), 8.07-7.99 (m, 4H), 4.42 (s, 2H). This spectrum is
375 identical to the reported one.^[27]

376 ***N*-Pyren-1-yl-2-(1,4,8,11-tetraazacyclotetradec-1-yl)-acetamide (L)**. This ligand was synthesized
377 according to a reported method with slight modifications.^[17] Under an Ar atmosphere, a mixture of
378 cyclam (3.25 g, 16.2 mmol), 2-chloro-*N*-pyren-1-yl-acetamide (2) (940 mg, 3.2 mmol), K₂CO₃
379 (2.24 g, 16.2 mmol) and KI (270 mg, 1.6 mmol) in CH₃CN (677 mL) was heated under reflux.
380 After 24 h, the solvent was evaporated under reduced pressure and the residue was washed with
381 water and ether several times. The crude product was dried under vacuum overnight to yield the
382 product as an off-white powder which was used for the next step without further purification (1.46
383 g, 94%). ¹H NMR (CDCl₃) δ 11.4 (br s, 1H), 8.27 (d, *J* = 9.3 Hz, 1H), 8.19-7.96 (m, 8H), 3.44 (s,
384 2H), 2.90 (t, *J* = 5.4 Hz, 2H), 2.80 (m, 8H), 2.42 (t, *J* = 5.1 Hz, 2H), 2.3 (t, *J* = 5.1 Hz, 2H), 2.12 (m,
385 2H), 1.95 (m, 2H), 1.49 (m, 2H). This spectrum is identical to the reported one.^[17]

386 **Complex [Ni^{II}(Cl)(L)]Cl (1)**. A solution of **L** (100 mg, 0.11 mmol) in EtOH (2 mL) was added
387 dropwise to a solution of NiCl₂·6H₂O (52 mg, 0.11 mmol) in EtOH (2 mL). The pale green solution
388 turned immediately to orange then dark pink. After 3h at room temperature, the solvent was
389 evaporated to dryness and the blue-pink solid was dissolved in EtOH (6 mL) and ether was allowed
390 to slowly diffuse to this solution to give complex **1** as a pink-purple powder (78 mg, 61%). UV-Vis
391 [DMF]: λ nm (ε, M⁻¹ cm⁻¹): 543 (10.7), 389 (1880), 353 (10920), 343 (15000), 329 (10000), 277
392 (16300), 266 (11060).

393 Single crystals suitable for X-ray diffraction were obtained by slow diffusion of Et₂O into a solution
394 of DMF containing **1** at room temperature. CH₃CN, EtOH and CH₂Cl₂ were also used instead of
395 DMF giving suitable single crystals. CCDC 2021920 (*trans*-**1**, MeCN), 2021925 (*trans*-**1**, EtOH),
396 2021922 (*trans*-**1**, DMF), 2021923 (*trans*-**1**, DCM), 2021921 (*cis*-**1**, EtOH) and 2021924 (*cis*-**1**,
397 DMF) contain the supplementary crystallographic data for this paper.

398

399 *Homogeneous Electrochemical Studies*

400 All electrochemical experiments were performed on a VSP300 potentiostat (Bio-Logic Science
401 Instruments SAS) and were conducted at room temperature in *N,N*-Dimethylformamide (DMF). 0.1
402 M tetrabutylammonium hexafluorophosphate (TBAPF₆) was used as the supporting electrolyte. The
403 cyclic voltammetry (CV) experiments were carried out in a three electrode setup, with a 3 mm
404 diameter glassy carbon (GC) electrode as a working electrode, which was polished on a polishing
405 cloth with a 1 μm diamond suspension (Struers), sonicated for 10 seconds, thoroughly rinsed with
406 ethanol and dried prior to experiments. Platinum wire was used as a counter electrode and was
407 previously flame annealed. The reference electrode was an Ag/AgCl electrode in a saturated KCl
408 solution, equipped with a bridge to allow operation in organic solvent. All potentials were calibrated
409 using the ferrocene/ferrocenium (Fc⁺⁰) redox couple as an internal standard, which was added in
410 solution at the end of each measurement. In DMF, E_{1/2} (Fc⁺/Fc⁰) = 0.60V vs Ag/AgCl/sat. KCl.
411 Only the second cycle of all CVs are shown, although no difference in consecutive scans has been
412 observed.

413 Controlled potential electrolysis (CPE) experiments were carried out in a gas-tight two-
414 compartment electrochemical cell with two ceramic-PVDF composite membranes (16 μm
415 thickness, Xuran) separating the anodic and cathodic compartments. The working electrode was a 1
416 cm² glassy carbon plate, the counter electrode was a platinum mesh and the reference electrode was
417 an Ag/AgCl electrode in a saturated KCl solution, equipped with a bridge to allow operation in
418 organic solvent. Anolyte and catholyte contained DMF and 2 M of H₂O as the proton source and
419 0.1 M of TBAPF₆ as the electrolyte. Only in the catholyte 1 mM of complex **1** was added. Both
420 solution compartments were saturated with CO₂ during at least 20 minutes before starting the
421 electrolysis, but no more gas was bubbled during the electrolysis. The experiments were conducted
422 at room temperature under stirring at the cathode side. The volume of solution held by the cell in
423 total was 22.6 mL, with ca. 10.6 mL of total headspace volume.

424 Gas products were quantified by gas chromatography (Model 8610C SRI Instruments) equipped
425 with TCD and FID detectors from 50 μL aliquots of the headspace of the cathode compartments.
426 Hydrogen (H₂) and carbon monoxide (CO) were detected by thermal conductivity detector (TCD)
427 and flame ionization detector (FID), respectively. Liquid products were evaluated using an ionic
428 exchange chromatograph (Metrohm 883 Basic IC) equipped with a Metrosep A Supp 5 column and
429 a conductivity detector.

430 The faradaic yields were calculated by quantifying the products in the head-space gas of the
431 cathodic side, on the basis of Equation 1:

432
$$\text{Faradaic efficiency} = \frac{N \times F \times n}{Q} \times 100 \quad (1)$$

433 Where Q , F , and N represented the charge passed through the system (C), Faraday's constant (C
434 mol⁻¹), and moles of H₂/CO generated, respectively. In the reaction process, 2 moles of electrons
435 were consumed to produce 1 mole of product, therefore $n = 2$.

436

437 *Electrodes preparation and characterization*

438 The electrodes used a 3 cm x 1 cm gas diffusion layer (GDL, AVCarb GDS 3250, Fuel Cell Store)
439 strip, which was briefly sonicated in EtOH and let dry in air before utilization. MWCNTs (Sigma)
440 were used after acid treatment as following: the raw MWCNTs material were dispersed in H₂SO₄ (2
441 M), sonicated for 1 h at ambient temperature, washed repeatedly with H₂O, then EtOH and dried in
442 a vacuum oven at 70°C overnight. This acid treated MWCNTs (2 mg) were sonicated for at least 30
443 min in EtOH (200 μl) containing a solution of Nafion perfluorinated resin (5 μl of a 5 wt% solution
444 in mixture of lower aliphatic alcohols containing 5% water). The suspension was then drop-casted
445 on the GDL (1 cm² deposit) and dried in air at 70°C for at least 30 min. Subsequently, the GDL-
446 MWCNT electrode was immersed in a solution of complex **1** in DMF (10 mM) overnight on an
447 orbital shaker at low speed. Finally, the electrode was dried, washed with water then acetonitrile
448 and dried in air.

449 SEM images were acquired using a Hitachi S-4800 scanning electron microscope. X-ray
450 photoelectron spectra (XPS) were collected using a Thermo Electron Escalab 250 spectrometer with
451 a monochromated Al K α radiation (1486.6 eV). The analyzer pass energy was 100 eV for survey
452 spectra and 20 eV for high resolution spectra. The analysed area was 500 mm². The photoelectron
453 take-off angle (angle between the surface and the direction in which the photoelectrons are
454 analysed) was 90°. Curve fitting of the spectra was performed with the Thermo Electron software
455 Advantage. The electroactive sites were calculated through the integration of the oxidation wave in
456 the CV scan (Figure S9) according to Equation 2:

$$457 \quad \Gamma Ni = \frac{q}{nFA} \quad (2)$$

458 Where ΓNi is the number of electroactive sites (mol cm⁻²), q is the charge (C) obtained from the
459 integration of the oxidation wave, n the number of electrons in the redox process per Ni center ($n =$
460 1), F is the Faraday constant (96485 C mol⁻¹), and A is the geometrical electrode area (1 cm²).^[13]

461

462 *Heterogeneous Electrochemical Studies*

463 Linear sweep voltammetry (LSV) was performed for each sample before CPE, first under Ar and
464 successively under CO₂. Gas was bubbled in the solution for at least 20 minutes before each
465 experiment. The scan rate was 10 mV s⁻¹. CPE experiments were carried out in a gas-tight H-shape

466 cell in which cathode and reference electrode are separated from the anode by an anion exchange
467 membrane (AMV Selemion, ACG Engineering). The solvent used was acetonitrile containing 1%
468 of H₂O, and the electrolyte was TBAPF₆ 0.1 M. The cathode used was a GDL on which MWCNs
469 with the complex **1** were drop-casted as described above, the anode was platinum and the reference
470 electrode was an Ag/AgCl electrode in a saturated KCl solution, equipped with a bridge to allow
471 operation in organic solvent. All potentials were calibrated using the ferrocene/ferrocenium (Fc⁺⁰)
472 redox couple as an internal standard, which was added in solution at the end of each measurement.
473 In acetonitrile, E_{1/2}(Fc⁺/Fc⁰) = 0.54V vs Ag/AgCl/sat. KCl. CO₂ gas was bubbled in the solution for
474 at least 20 minutes before each experiment and no more gas was bubbled during the electrolysis.
475 The experiments were conducted at room temperature and under stirring at the cathode side. The
476 volume of solution held by the cell in total was 22.6 mL, with ca. 10.6 mL of total headspace
477 volume.

478 The electrolysis products (hydrogen, CO and formate) were quantified in a similar manner as in the
479 homogeneous electrochemical studies part. The faradaic yields were calculated by quantifying the
480 products in the head-space gas of the cathodic side, on the basis of Equation 1 (see above).

481 The following formulas

$$482 \quad TON = \frac{\text{moles of product}}{\text{moles of catalyst}} \quad (3)$$

483 and

$$484 \quad TOF = \frac{TON}{\text{reaction time [s]}} \quad (4)$$

485 were used to calculate Turnover Number (TON) and Turnover Frequency (TOF) values,
486 respectively.

487

488 **Acknowledgements**

489 *S.P. and D.G. acknowledge financial support from the European School on Artificial Leaf:*
490 *Electrodes & Devices (eSCALED). This project has received funding from the European's Union's*
491 *Horizon 2020 research and innovation programme under the Marie Skłodowska-Curie grant*
492 *agreement No 765376.*

493 *We thank Geoffrey Gontard (Sorbonne Universités) for solving the structure of cis-1 (DMF).*

494 *We thank Françoise Pillier (Sorbonne Universités) for the SEM images.*

495

496

497 **References**

498

- 499 [1] A. Liu, M. Gao, X. Ren, F. Menga, Y. Yang, L. Gao, Q. Yang, T. Ma, *J. Mater. Chem. A.*
500 **2020**, *8*, 3541–3562.
- 501 [2] B. Kumar, J. P. Brian, V. Atla, S. Kumari, K. A. Bertram, R. T. White, J. M. Spurgeon, *Catal.*
502 *Today* **2016**, *270*, 19–30.
- 503 [3] D. Gao, F. Cai, G. Wang, X. Bao, *Curr. Opin. Green Sustain. Chem.* **2017**, *3*, 39–44.
- 504 [4] R. Francke, B. Schille, M. Roemelt, *Chem. Rev.* **2018**, *118*, 4631–4701.
- 505 [5] K. Elouarzaki, V. Kannan, V. Jose, H. S. Sabharwal, J. M. Lee, *Adv. Energy Mater.* **2019**, *9*.
- 506 [6] N. Elgrishi, M. B. Chambers, X. Wang, M. Fontecave, *Chem. Soc. Rev.* **2017**, *46*, 761–796.
- 507 [7] C. Sun, R. Gobetto, C. Nervi, *New J. Chem.* **2016**, *40*, 5656–5661.
- 508 [8] L. Sun, V. Reddu, A. C. Fisher, X. Wang, *Energy Environ. Sci.* **2020**, *13*, 374–403.
- 509 [9] X. M. Hu, M. H. Rønne, S. U. Pedersen, T. Skrydstrup, K. Daasbjerg, *Angew. Chemie - Int.*
510 *Ed.* **2017**, *56*, 6468–6472.
- 511 [10] Y. Wu, Z. Jiang, X. Lu, Y. Liang, H. Wang, *Nature* **2019**, *575*, 639–642.
- 512 [11] X. Zhang, Y. Wang, M. Gu, M. Wang, Z. Zhang, W. Pan, Z. Jiang, H. Zheng, M. Lucero, H.
513 Wang, G. E. Sterbinsky, Q. Ma, Y. Wang, Z. Feng, J. Li, H. Dai, Y. Liang, *Nat. Energy*
514 **2020**.
- 515 [12] J. D. Blakemore, A. Gupta, J. J. Warren, B. S. Brunshwig, H. B. Gray, *J. Am. Chem. Soc.*
516 **2013**, *135*, 30.
- 517 [13] B. Reuillard, K. H. Ly, T. E. Rosser, M. F. Kuehnel, I. Zebger, E. Reisner, *J. Am. Chem. Soc.*
518 **2017**, *139*, 14425–14435.
- 519 [14] P. Kang, S. Zhang, T. J. Meyer, M. Brookhart, *Angew. Chemie - Int. Ed.* **2014**, *53*, 8709–
520 8713.
- 521 [15] G. Neri, J. J. Walsh, C. Wilson, A. Reynal, J. Y. C. Lim, L. Xaoe, A. J. P. White, N. J. Long,
522 J. R. Durrant, A. J. Cowan, *Phys. Chem. Chem. Phys.* **2015**, *17*, 1562–1566.
- 523 [16] A. Zhanaidarova, C. E. Moore, M. Gembicky, C. P. Kubiak, *Chem. Commun.* **2018**, *54*,
524 4116–4119.
- 525 [17] N. J. Youn, J. S. Kim, K. C. Song, S. H. Kim, S. Ahn, S. K. Chang, *Bull. Korean Chem. Soc.*
526 **2005**, *26*, 849–851.
- 527 [18] Y. Zhao, D. Xue, H. Qi, C. Zhang, *RSC Adv.* **2017**, *7*, 22882–22891.
- 528 [19] J. D. Froehlich, C. P. Kubiak, *Inorg. Chem.* **2012**, *51*, 3932–3934.
- 529 [20] J. D. Froehlich, C. P. Kubiak, *J. Am. Chem. Soc.* **2015**, *137*, 3565–3573.
- 530 [21] C. Costentin, M. Robert, J.-M. Savéant, *Chem. Soc. Rev.* **2013**, *42*, 2423–2436.
- 531 [22] S. Creager, *Handbook of Electrochemistry*, ed. C. Zoski Elsevier, Amsterdam, **2007**, p.101.
- 532 [23] P. D. Tran, A. Le Goff, J. Heidkamp, B. Jousset, N. Guillet, S. Palacin, H. Dau, M.
533 Fontecave, V. Artero, *Angew. Chemie - Int. Ed.* **2011**, *50*, 1371–1374.

- 534 [24] T. Qiu, G. P. A. Yap, J. Rosenthal, *ACS Appl. Energy Mater.* **2019**, *12*, 8560–8569.
- 535 [25] M. Beley, J. P. Collin, R. Ruppert, J. P. Sauvage, *J. Am. Chem. Soc.* **1986**, *108*, 7461–7467.
- 536 [26] Y. Wu, B. Rudshiteyn, A. Zhanaidarova, J. D. Froehlich, W. Ding, C. P. Kubiak, V. S.
537 Batista, *ACS Catal.* **2017**, *7*, 5282–5288.
- 538 [27] J. H. Kim, A. R. Hwang, S. K. Chang, *Tetrahedron Lett.* **2004**, *45*, 7557–7561.
- 539